Optimal Finned Heat Sinks

William R. Hamburgen

28 October 1986

Digital Equipment Corporation
Western Research Laboratory
100 Hamilton Avenue
Palo Alto, CA 94301

Abstract

In a multi-board computer system, the volume allocated for heat removal is often a significant fraction of the total system volume. Cooling requirements can thus impact performance, reliability, cost, acoustic noise, and floorspace. This work addresses the volume costs or space requirements for removing heat with optimally designed finned heat sinks. Simple formulas applicable to both gas and liquid cooling problems provide upper bounds on the thermal resistance of an optimal heat sink, without explicitly designing the part. Conservative junction temperature estimates can thus be made without detailed design.

Preface

The design of electronic circuits is usually limited by one or more limited fundamental resources. For example, the area of a circuit board or the area of an integrated circuit is a fundamental resource.

In multi-board processors, *volume* is a fundamental resource. Volume is needed to remove heat from circuits as well as to store the components. Volume is often the most important limit: cooling requirements typically force larger module-to-module spacings than would be otherwise desired. The longer signal paths that result from this increased spacing can reduce computational speed. Even in systems where there is no direct performance penalty, the volume used for cooling affects costs, reliability, noise levels, and floorspace, and thus influences customer acceptance.

This report describes research work into the volume costs or space requirements for removing heat with optimally-designed finned heat sinks. The solutions presented are very general in nature, and can be applied to both gas and liquid cooling problems. The general approach is to assume a fluid at some velocity flowing through a heat sink of a given material and specified outline dimensions (Figure 1). It evaluates both non-ducted or open-finned heat sinks (as shown) and the more complicated capped or ducted heat sinks. For the system designer, there are simple formulas that give conservative upper bounds on the thermal resistance of optimal heat sinks, without the necessity of individually designing them (see example in Section 3.8).

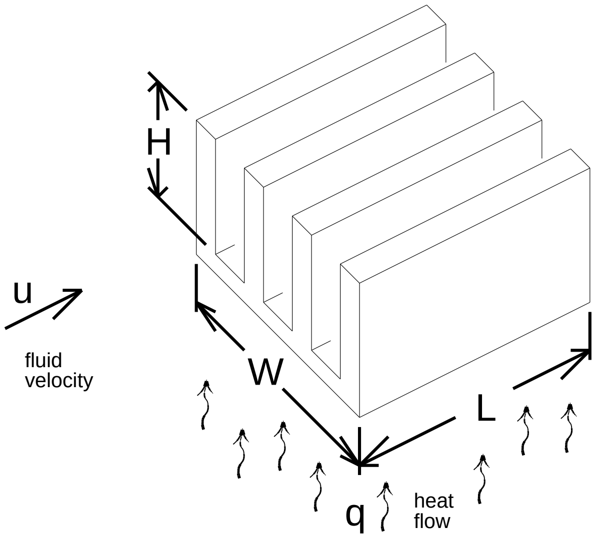

Figure 1: Heat Sink of Specified Outline Dimensions

This information is useful both to system designers and to thermal engineers. Each will appreciate the closed-form optimizations that permit the comparisons of possible systems without requiring detailed heat sink design and analysis. The thermal engineer will additionally benefit from the the lossless-fin analysis, the non-ducted fin-spacing optimization, and the Nusselt number substitution that permits a unified approach to optimizing both ducted (enclosed fin) and non-ducted designs.

It is not necessary to be familiar with heat transfer or fluid mechanics to understand this material, and the report presents enough background material that a non-specialist can use and understand the models, and can even develop intuitions for their use. A number of examples demonstrate practical applications.

Thermal engineers will find enough detail to be able to verify, adapt, and extend the theory. Further work is needed on understanding onset of turbulence and wake effects, more accurately determining optimal non-ducted fin spacing, obtaining an exact fin-thickness optimization, and extending the results for tower heat sinks.

1

Introduction and Overview

This chapter introduces the reader to the theory of heat transfer and fluid mechanics, to a level of detail sufficient to understand and apply the results in the remainder of this paper. The presentation of the theory borrows heavily on the introductory material from Tuckerman [15, pp. 9-15], and will be brief and appeal to intuition. A more detailed exposition may be found in Holman [6, p. 161] or Kays and Crawford [7].

In subsequent chapters we will study two particular types of straight-finned heat sinks, ducted and non-ducted. Non-ducted designs are exemplified by traditional forced-air computer cooling. The fluid is directed through the space between the circuit boards, but is not explicitly constrained to flow through the fins of any heat sinks that happen to be present. Digital's VAX 8xxx series computers and air-cooled motorcycles provide examples of non-ducted fin arrays. In ducted heat sinks, the fluid is channeled directly over the fins, its path confined and controlled by surrounding shrouding. The water-cooled coldplate used in IBM 30xx series computers and the air-cooled motor of the VW Beetle are examples of ducted designs. Partially ducted variants are also possible. It will be shown that for a given heat sink, there is some transition velocity above which it is irrelevant whether or not the flow is ducted. For lower velocities however, the presence of ducting has a profound effect. The next few sections set the stage for understanding this and related phenomena.

1.1 Heat Conduction

Heat may be transported by one of three means: radiation, conduction, or convection. Radiation is too inefficient to be useful in cooling dense circuitry near room temperature, and will not be considered further. Heat conduction is described by Fourier's Law. For one-dimensional steady-state conduction through a body of constant cross section, Fourier's Law reduces to:

$$q = \frac{kA\Delta T}{H} \tag{1}$$

where:

q = heat flow (total heat-transfer rate), W
k = thermal conductivity, W/(m °C)
A = area normal to the direction of heat flow, m^2
ΔT = temperature difference (across height H), °C
H = height in direction of heat flow, m

For example, in axial conduction through a rod, the temperature difference between the ends of the rod ΔT is the driving function. The heat flow q is proportional to the material's thermal conductivity k and the rod's cross-sectional area $A = \pi \cdot radius^2$. The heat flow is inversely proportional to the rod's height H.

While it may not be obvious at first glance, convection is simply conduction in a moving fluid, so the physics are essentially those of a conduction process. Convection is conventionally expressed in much the same form as Fourier's Law with the length H and the thermal conductivity k replaced by a convection coefficient h. The magnitude of h depends on the flow geometry as well as the fluid's velocity and physical properties.

$$q = hA_h\Delta T \tag{2}$$

where:

h = convection coefficient, W/(m^2 °C)
A_h = surface area for convection, m^2
ΔT = temperature difference between surface and bulk fluid, °C

For example, in convection from one side of a square plate, the temperature difference between the passing fluid and the surface of the plate ΔT is the driving function. The heat flow q is proportional to the plate's average convection coefficient h and its surface area $A_h = side^2$.

1.2 Components of Thermal Resistance

The performance of a convective heat-transfer system for integrated circuits is measured by its thermal resistance,

$$\theta = \frac{\Delta T}{q} \tag{3}$$

where:

θ = thermal resistance, °C/W
ΔT = temperature rise of the circuit above ambient, °C
q = integrated-circuit power dissipation, W

This formalism is useful when θ is independent of temperature, which is a good approximation in forced-convection cooling systems. It can also be applied to portions of a system. This allows combining series and parallel thermal resistances in the same manner as Ohm's law allows combining electrical resistances. Here the temperature rise ΔT can be considered analogous to voltage and the thermal power dissipation q can be considered analogous to the electrical current. Thermal resistance for both convection and one-dimensional conduction can be conveniently expressed in this form:

$$\theta_{convection} = \frac{1}{hA} \tag{4}$$

and,

$$\theta_{conduction} = \frac{H}{kA}$$

where:

$\theta_{convection}$ = convection thermal resistance, °C/W
$\theta_{conduction}$ = conduction thermal resistance, °C/W

For cooling integrated circuits in single-chip packages, θ can be considered the sum of four components: θ_{j-c}, the resistance between the individual semiconductor junctions and the outside of the package; $\theta_{interface}$, the thermal resistance associated with the package to heat sink interface (if any); $\theta_{heatsink}$, the thermal resistance between the heat sink and the coolant fluid; and $\theta_{caloric}$, the caloric thermal resistance due to the heating of the fluid as it absorbs energy passing through the heat sink.

The first of these components, θ_{j-c} is determined by the chip package and die attach and so is usually not under the direct control of the system designer and will not be considered further here. The interfacial resistance $\theta_{interface}$, is determined by the characteristics of the bond between the heat sink and the package. In addition to thermal resistance requirements, its design is often subject to manufacturing constraints and the need for endurance in thermal cycling; such details are beyond the scope of this paper.

The thermal resistance between the heat sink and the fluid ($\theta_{heatsink}$) and its minimization subject to volume and velocity constraints, are the primary focus of this paper and will be treated in some detail. It can generally be regarded as the sum of a conduction thermal resistance through the heat sink fins and a convection thermal resistance to the passing fluid. The conduction through the fins can be easily analyzed with Fourier's Law; convection is a bit more complicated and will be examined in the next few sections.

The caloric thermal resistance $\theta_{caloric}$ has a very simple form:

$$\theta_{caloric} = \frac{1}{\rho c_p f} \tag{5}$$

where:

ρc_p = volumetric heat capacity of the fluid, (W sec)/(m^3 °C)]
ρ = density, kg/m^3
c_p = heat capacity, (W sec)/(kg °C)
f = volume flow rate, m^3/sec

$\theta_{caloric}$ can be made small by using fluids with a high volumetric heat capacity (such as liquids) or using a high flow rate. Caloric resistance is not often a significant term in liquid cooled systems, but can become important with gases. For example, note that ρc_p for water is about 4000 times that of air (see Table D-1). This can be particularly important when air traverses a number of heat sinks in series, each device progressively raising the temperature of the passing gas. Even when the heat sinks receive their air in parallel, with particularly effective heat sinks it is possible that $\theta_{caloric}$ will be greater than $\theta_{heatsink}$. Since the impact of the caloric resistance depends on details of the particular system under consideration, it is not explicitly evaluated in the coming heat sink optimizations. It must, however, be evaluated by the system designer.

1.3 Entrance-Region Heat-Transfer Theory

The thermal resistance between a finned heat sink and the fluid ($\theta_{heatsink}$) can be regarded as the sum of a resistance due to conduction within the fins and a resistance due to convection to the passing fluid. The heat transport through the fins can be analyzed by applying Fourier's conduction law. The analysis of the conduction from the fin to the fluid requires an understanding of how heat is convected.

Real fluids have finite viscosity. They resist deformation. This has a profound effect on convective heat transfer. When a fluid having a free-stream velocity of u flows past a solid surface or wall, such as a flat plate or the inside of a pipe, the fluid velocity is constrained by viscosity to be zero at the wall. The velocity therefore varies from zero at the wall to u far from the wall. The region near the wall where the majority of this transition occurs is called the momentum boundary layer. The boundary-layer thickness increases as one moves downstream until its growth is constrained by another nearby wall, as in laminar pipe flow or by the mixing action of turbulent eddies, as in turbulent flow. A flow is considered laminar if it is free of the these random eddies. The importance of the boundary layer can be understood by considering a hypothetical fluid with zero viscosity. In such a case there would be no boundary layer. The fluid adjacent to the wall would pass at the free- stream velocity and as will be shown, the convective thermal resistance would be zero!

The region where boundary-layer growth is unconstrained by turbulent eddies or another wall is called the *entrance region*. Predicting where entrance-region conditions will be encountered will be discussed in Sections 1.5 and 2.5. Inside the boundary layer there is a velocity gradient, the velocity reaching zero at the wall. Outside the entrance-region boundary layer, free-stream conditions exist; the fluid proceeds at its original velocity. The edge of the boundary layer is typically defined as a locus of points where the velocity is a given fraction of the free-stream value. Its thickness in the entrance region can be expressed in the form:

$$\delta = \gamma \sqrt{\nu}\,\sqrt{x/u} \qquad (6)$$

where:

δ = momentum boundary-layer thickness, m
γ = boundary-layer thickness parameter, dimensionless
ν = kinematic viscosity, m^2/sec
x = distance from the leading edge of the plate, m
u = free-stream velocity, m/sec

Figure 1-1 shows such an entrance-region boundary layer over a thin flat plate. The same drawing could just as well depict the entrance of a thin wall pipe; the leading edge of a plate is indistinguishable from the entrance to a pipe of large diameter. The value of the constant γ is determined by the specifics of how one chooses to define boundary-layer thickness. Having an appropriate value for γ is important to an engineer who wants to optimize non-ducted heat sinks (Section 2.7), but it is not necessary for understanding the mechanisms of convection.

An intuitive understanding of convective heat transfer from a plate to a passing fluid can be gained by considering the entire boundary layer to be stagnant (that is, stationary with respect to the wall). The convection problem can then be viewed as a stationary conduction problem; heat from the plate conducts through the stagnant boundary layer to the passing fluid. Since the resistance to heat flow is proportional to the boundary-layer

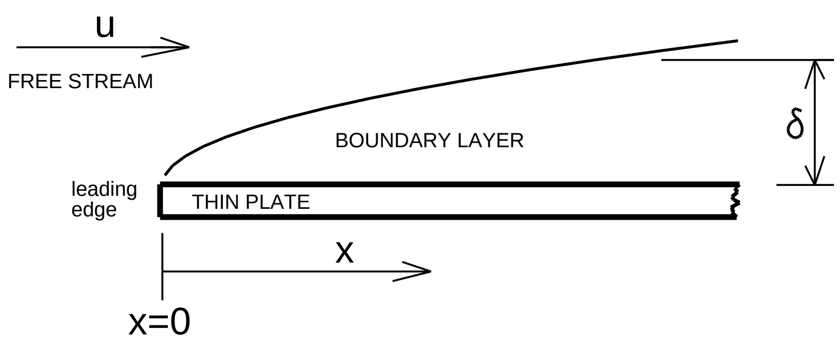

Figure 1-1: Boundary Layer on a Semi-Infinite Flat Plate

thickness, the resistance will be lowest for small *x*. This is an important point; heat transfer to a passing fluid is highest where the fluid first encounters an object. This is true even for geometries other than flow entering a pipe or parallel to a flat plate. In impingement cooling for example, a jet of coolant from a hole or slot impacts a surface at right angles, turning and heading away from the point of impact. As would be expected, heat transfer is highest near the point of impact, where the boundary layer is thinnest.

A more detailed analysis verifies our intuition; the ratio $\sqrt{u/x}$ occurs precisely as equation (6) and our stagnant boundary-layer assumption had led us to expect [6].

$$h_x = 0.332 \frac{k_s \sqrt[3]{\mathrm{Pr}}}{\sqrt{\nu}} \cdot \sqrt{u/x} \tag{7}$$

where:

h_x = local convection coefficient, W/(m^2 °C)
Pr = $\nu\rho c_p / k_s$ = Prandtl number, dimensionless
k_s = fluid thermal conductivity,W/(m °C)

The local convection coefficient in the entrance region, h_x, is given in terms of the Prandtl number, a convenient dimensionless group that relates the dynamic and thermal properties of the fluid*. It is found universally in correlations for both laminar and turbulent flow.

While the entrance-region heat-transfer model was based on a semi-infinite plate of infinitesimal thickness, reasonable agreement is obtained with tests on plates of finite

*A dimensionless group is not a physical quantity but rather a way of characterizing or understanding other physical quantities. We introduce new dimensionless-group names when it is convenient to do so. While this increases the reader's ''variable-name overhead'' somewhat, the relations tend to be easier to understand, and valuable insights may be gained. Also, it is noble to remember the dead European physicists for whom the numbers are named.

dimensions. We will apply this heat-transfer model in Section 2.8 to the design of optimal heat sinks.

Equation (7) can be used to define a thermal boundary layer whose thickness may be different that of the momentum boundary layer defined in equation (6). The degree of mismatch will depend on the fluid's Prandtl number Pr, and on the choice of the boundary-layer thickness parameter γ. Also, the derivation of equation (7) assumed that the Prandtl number of the fluid is greater than 1. While air and most other gases have Prandtl numbers somewhat less than one, the model is still quite accurate. Some of the ramifications of this are explored in Appendix B.

1.4 Fully-Developed-Region Heat-Transfer Theory

If one follows a pipe or channel flow downstream well past the point where neighboring walls begin interfering with boundary-layer growth, a region of fully-developed flow is reached. In this region, the fluid has asymptotically approached a fully-developed velocity and temperature profile and the heat-transfer coefficient has reached its minimum value. In a region where the convection coefficient is unvarying, it can be most conveniently defined in terms of a Nusselt number. This dimensionless number is useful since it depends only on the shape of the duct and the thermal boundary conditions, and not on the duct size or the fluid used.

$$h_d = \frac{k_s \mathrm{Nu}_d}{d} \tag{8}$$

where:
h_d = convection coefficient, W/(m^2 °C)
Nu_d = duct Nusselt number, dimensionless
d = duct hydraulic diameter, m

The duct hydraulic diameter is another useful construct. Because of its axial symmetry, which facilitates analysis, the circular duct or pipe has been chosen as a base case. Ducts of arbitrary section are correlated to the base case by their cross-sectional area and wetted perimeter (interior outline of the duct), according to the following convention:

$$d = 4 \cdot \frac{cross\text{–}sectional\ area}{wetted\ perimeter} \tag{9}$$

Note that in the case of a round pipe, the inside diameter equals the hydraulic diameter. On ''nearly round'' sections, good agreement is obtained by using equation (9) and the circular-duct laminar-flow Nusselt number of $\mathrm{Nu}_d = 4.364$. For many shapes that are not ‘‘nearly round’’, numerical solutions for Nu_d have been obtained. Nusselt numbers for laminar flow in rectangular ducts are found in Tuckerman [15] and the relevant data included here as Appendix C. Our interest here is finned heat sinks; these can be modeled as sets of parallel-plate ‘‘pipes’’ with opposite walls a distance s apart. In the case where the length of the leading edge is much greater than the fin gap s, by equation (9) we have,

$$d = 2s \tag{10}$$

where: s = space between fins or walls, m

In this case Nu_d approaches 8.235, thus we approximate:

$$h_d = \mathrm{Nu}_d \frac{k_s}{2s} = \frac{8.235\, k_s}{2s} \tag{11}$$

As we might expect, the convection coefficient in fully-developed flow increases with increasing fluid conductivity. The coefficient also increases as the channel width is reduced. In smaller channels the passing fluid is ‘‘closer’’ to the walls, which suggests a lower convection coefficient. It is worth noting that h_d is independent of the fluid velocity u in this regime. Varying the velocity will change the caloric thermal resistance but the convection term will remain unchanged.

1.5 Turbulent Flow

We have thus far examined entrance-region heat transfer, where boundary-layer growth is unconstrained, and fully-developed region heat transfer, where boundary-layer growth is constrained by an opposing wall. We’ll now take a brief look at the third possibility: turbulent flow. In turbulent flow, the growing boundary layer is constrained by the mixing action of turbulent eddies. This improves the heat transfer beyond that predicted by the entrance-region and fully-developed models. The inherent disorder in turbulent flow makes analysis difficult and empirical correlations are typically relied upon. While an examination of turbulent-flow heat transfer is beyond the scope of this paper, we will look at criteria for determining when a heat sink is likely to be operating in this regime and how much of the fin is affected.

Whether or not the laminar entrance-region flow or a fully-developed laminar pipe flow is likely to be disrupted by turbulence can be determined by an examination of the Reynolds number. Reynolds number is yet another dimensionless group. It takes the form,

$$\mathrm{Re} = \frac{dim\, u}{\nu} \tag{12}$$

where:

Re = Reynolds number, dimensionless
dim = characteristic dimension, m
u = free-stream velocity, m/sec
ν = kinematic viscosity, m^2/sec

The flow is presumed laminar if the Reynolds number is less than some critical value; above this critical value begins a gradual transition to a fully-turbulent flow. The characteristics are summarized below.

TRANSITION TO TURBULENT FLOW		
Flow type	Characteristic dimension	Flow is Laminar if
Pipe or duct	$dim = d = 2\,s =$ duct equiv. diameter	Re < 2100
Entrance region or flat plate	$dim = x =$ distance from leading edge	Re < 500 000

These numbers are guidelines, not absolute truth. For example, in plate flow with large disturbances in the incoming stream, the transition may begin as low as $\mathrm{Re} = 10^5$, and for flows that are very free from fluctuations, turbulence may not start until $\mathrm{Re} = 2 \cdot 10^6$ or more [6]. Similar variations are found with pipe flows.

There are additional uncertainties. As fluid enters a duct, the edge of the duct looks to the fluid much like the edge of a flat plate and the flat-plate Reynolds number can be expected to apply. Farther down the duct, if it is sufficiently long, the developing boundary layers join and approach a constant profile. Here duct Reynolds numbers can be expected to apply. Surprisingly, other authors have applied duct Reynolds numbers to predict the onset of turbulence even with very short ducts when the boundary layers did not meet and plate Reynolds numbers indicated a laminar boundary layer [9]. Use of the duct Reynolds number on very short ducts may indicate turbulence where none is present. A better understanding of onset of turbulence is needed.

While turbulent flow is associated with higher heat-transfer rates than laminar flow, the entrance-region laminar-flow model can provide a conservative first approximation even where turbulence might be expected over a portion of the fin surface. In cases where the comparison has been made, the entrance-region laminar model underestimates the convection coefficient by no worse than a factor of two, and is typically quite a bit closer [9, 18]. This has important implications to the system designer; use of laminar-flow models is conservative and will result in safe junction temperatures even when turbulence is present.

Example: Air flows over a plate at 5 m/sec (about 1000 fpm). How far from the leading edge of the plate do we expect onset of turbulent flow?

Material properties for air are found in Appendix D. The transition Reynolds number for a flat plate is $\mathrm{Re} = 5{\cdot}10^5$. Solving equation (12) for *dim* gives:

$$dim = \mathrm{Re}\frac{\nu}{u} = (5{\cdot}10^5)\frac{16.8{\cdot}10^{-6}}{5.0} = 1.68\,\mathrm{m}\ (.66'')$$

This distance is large compared to the dimensions typically encountered in electronic assemblies, even at this high velocity. On the basis of this computation, we would not expect turbulent flow over the fin of a non-ducted heat sink.

Example: Air flows between two long circuit boards at 5 m/sec. How far apart can the boards be spaced without onset of turbulence?

The transition Reynolds number for duct is $\mathrm{Re} = 2100$. Solving again for *dim* gives:

$$dim = (2100)\frac{16.8{\cdot}10^{-6}}{5.0} = 0.007\,\mathrm{m} = 7\ \mathrm{mm}\ (.28'')$$

Since the duct equivalent diameter is twice the board spacing, this corresponds to a board spacing of only 3.5 mm.

Since typical board spacings are larger than this, we can expect turbulent flow over at least the downstream portion of the boards in many air-cooled systems.

1.6 Applying Convection Theory to Heat Sinks

In the previous sections, we developed expressions for both entrance-region and fully-developed convection coefficients. To apply these models to heat sink optimization, some assumptions will have to be made. We assume that for ease of fabrication, the fins will be of a single uniform thickness. As will be seen, the optimal thickness of a flat fin represents a compromise between number of fins (hence surface area) and fin conduction losses. When the convection coefficient over the fin is uniform, selecting this thickness is straightforward. When the coefficient is not uniform, as is the case particularly in the entrance region, a choice must be made since the thickness chosen can be optimal only for some particular value of the convection coefficient. Two obvious possibilities are the minimum convection coefficient, which occurs near the trailing edge, or the average convection coefficient for the fin.

Choosing the minimum convection coefficient will yield a fin thickness that is optimal at the trailing edge. This will minimize the peak source temperature but compromise the heat transfer closer to the leading edge. It will also give the smallest temperature gradient across the base. This might be the most appropriate choice where a single heat sink cools a large multi-chip module. Choosing the average convection coefficient will yield a fin thickness that minimizes the average source temperature. This would be most appropriate for a typical single-chip package, particularly where there is an appreciable thickness of conductive material between the junctions and the base of the fins that will tend to equalize temperatures across the die. The choice is up to the analyst. Since we are interested primarily in single-chip packages, subsequent optimizations will be based on the average convection coefficient.

By integrating equation (7) over the length of the plate and dividing by *L*, we find that the average convection coefficient over a fin is twice the local coefficient at the trailing edge,

$$h_{L,average} = 0.664\,\frac{k_s\sqrt[3]{\mathrm{Pr}}}{\sqrt{\nu}}\cdot\sqrt{u/L} \tag{13}$$

where: $h_{L,average}$ = average plate convection coefficient, W/(m^2 °C)

A similar choice must be made in optimizing heat sinks where fully-developed flow is expected over most of the fin. While one could correct for the higher convection coefficient near the leading edge (entrance region), our subsequent optimizations will assume that flow is fully developed over the entire length of the duct. We will use the fully-developed value as our average convection coefficient. This is a good approximation where the entrance region is a small proportion of the total duct length. It is also a conservative choice. With the fin thickness optimized for the fully-developed portion, the actual $\theta_{heatsink}$ will be lower than predicted.

The formulas in this paper can also be used to design heat sinks for operation in the turbulent-flow regime, however determining the average convection coefficient in such cases is beyond the scope of this report.

1.7 Scope of this Report

The heat transfer theory outlined in the previous few sections is most of what an engineer needs to know to design optimal laminar-flow heat sinks. As explained above, the resistance $\theta_{heat\ sink}$ can be considered to be the sum of two terms: the resistance due to conduction along the fins, and the resistance due to convection to the coolant. To minimize $\theta_{heatsink}$, both the fin thickness and spacing must be correct. This process requires the allocation of a precious resource, volume, such that $\theta_{heatsink}$ is as small as possible. The following sections will show how to engineer this tradeoff.

The general approach is to assume a fluid flow of some velocity through a heat sink of some arbitrary material and outline dimensions. For such a fluid flow, we can compute the optimal fin spacing and thickness. This is done by first analyzing arrays of lossless or ideal fins, fins having zero thickness and infinite thermal conductivity. This gives a lower bound on the resistance of any real heat sink. A second lower bound is found by accounting for fin conductivity and thickness but assuming that fin length is unbounded. A pair of upper bounds are then developed that cover the same design space. The final step is a closed-form optimization that provides an upper bound over the whole space. This closed-form optimization permits conservative thermal performance estimates without requiring detailed heat sink design (see example in Section 3.8).

The approach has a number of benefits. For example, it is easy to determine how much a change in heat sink materials can affect thermal resistance. It is easy to determine whether or not fins will help, and why fins cannot help when the convection coefficient is too high and/or the fluid and fin thermal conductivities too similar. There is some discussion of when simple straight-fin structures are likely to be optimal and when the more complex tower-type heat sinks will yield a lower $\theta_{heatsink}$. There is an evaluation of the conditions under which there is a benefit to ducting or shrouding the flow to direct it through a fin array. This includes a surprising result for the non-ducted (unshrouded) lossless-fin case: the thermal resistance of an optimal non-ducted lossless-fin heat sink is independent of its length in the direction of flow, the resistance depends only on the heat sink's frontal area and the fluid velocity! A Nusselt number substitution is presented that permits direct comparison of ducted and non-ducted designs and a unified approach to optimizing both. There is also a brief examination of the performance of suboptimal non-ducted designs.

There are some important limitations to the applicability of this work. In many systems the fluid traverses a board to cool a number of identical heat sinks serially. When this is done, each heat sink will generally not exhibit identical performance. This phenomenon falls into the general class of periodic-developed flows; it may be a particularly significant effect in non-ducted designs. Our analysis also assumes incompressible flow;

it is applicable to gas flows only when pressure changes are small and at low Mach numbers**. Only flat fins are considered. While pin fins and other shapes may offer advantages in some regimes, they will not be discussed. Impingement cooling and its many variants are not discussed.

The cycle efficiency for the heat removal (watts of fluid power expended per watt of heat removed) is not directly evaluated in this report. The cycle efficiency can be important, but in many laminar-flow systems the heat sinks themselves contribute only minor losses to the total flow circuit. Also, for very fast computers, the energy efficiency is secondary to volumetric efficiency. For approaches that directly optimize thermal performance with respect to fluid power rather than velocity, refer to the dissertation by Tuckerman and to the 1984 article by Keyes [15, 8]. We will however show how the efficiency-optimal solutions of Tuckerman can be mapped into our velocity-optimal solutions.

**Mach number = flow velocity/speed of sound

2

Lossless-Fin Models

2.1 Introduction to Heat Sinks with Lossless Fins

In the previous chapter we showed how the heat sink thermal resistance $\theta_{heatsink}$, can be considered the sum of two terms: the resistance due to conduction along the fins, and the resistance due to convection to the coolant. To minimize this sum, both the fin thickness and spacing must be correct. This is essentially an allocation process for volume resources, such that $\theta_{heatsink}$ is as small as possible.

As a step toward understanding finned heat sink design, we first examine the case where the fins are lossless; that is where the fin material has an infinite thermal conductivity k. The infinite conductivity allows the fin thickness to go to zero. Volume resources can thus be dedicated entirely to convection, permitting optimization without regard for conduction losses. The lossless heatsink provides a useful bound on the performance of any real heat sink.

We first examine the basic lossless-fin heat sink and apply to it the fully-developed and entrance-region convection models from the previous chapter. Details of boundary-layer interaction are explored and used to find the limits of applicability of the two heat-transfer models. We show why both ducted and non-ducted heat sinks behave similarly in the high-velocity regime, but very differently below some transition velocity. An optimal fin-spacing criterion for non-ducted designs is derived and applied to the lossless-fin model. A Nusselt number substitution is defined that allows a unified treatment of both entrance-region and fully-developed designs. In subsequent chapters the lossless model will be extended to encompass the effects of finite-fin thermal conductivity. We then show how a large class of real heat sinks can approach the performance of the lossless designs.

2.2 Basic Lossless-Fin Model

A lossless heat sink is an array of fins having zero thickness and zero thermal resistance. Figure 2-1 depicts such a heat sink with fins spaced a distance *s* apart. To make them visible in the drawing, the fins were drawn with finite thickness *b*. There is no reason why they had to be shown as attached at right angles to the base. We can ignore the orientation of the fins (as long as they are parallel to the flow direction); since they have zero resistance, heat could presumably be supplied to each fin at any point. This is a powerful generalization that lets us consider the performance potential of a fin array without knowing the details of fin orientation. We can analyze a field of these ideal fins that completely fills an allotted volume, and use the analysis to calculate bounds on the performance of any real heatsink occupying the same space.

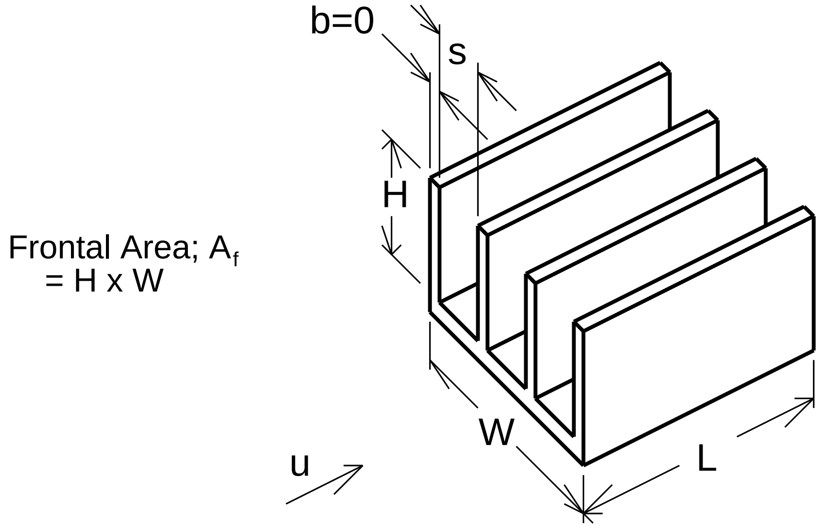

Figure 2-1: Heat Sink with Lossless Fins

It is useful to consider the bounding volume as the product of the frontal area A_f and the length L, where $A_f = H \cdot W$. The convection area or wetted area A_h of the heat sink is:

$$A_h = \frac{2 A_f L}{s} \tag{14}$$

where:

A_h = surface area for convection, m^2
$A_f = HW$ = frontal area, m^2
W = heat sink width, m
H = fin height, m
L = length of the fins in the direction of flow, m/sec
s = fin gap, m

Since by equation (4), $\theta = \frac{1}{hA}$, the thermal resistance of the lossless heat sink θ_{lossless}, is:

$$\theta_{lossless} = \frac{s}{2\,h_{average} L A_f} \tag{15}$$

where:
$\theta_{lossless}$ = thermal resistance of lossless heat sink, °C/W
$h_{average}$ = average convection coefficient, W/(m^2 °C)

Note that the thermal resistance of a lossless heat sink depends only on its volume $L \cdot A_f$, its fin gap s, and the average convection coefficient $h_{average}$.

2.3 Lossless Heat Sink in Fully-Developed Flow

The lossless model can be applied directly to the case of fully-developed flow. As was discussed in Section 1.6, this is the situation in which the entrance region comprises only a small proportion of the duct, and $h_{average}$ can be conservatively approximated by its asymptotic-minimum value. As will be seen, this model applies only to ducted structures at low velocities. By substituting equation (11) into equation (15) we have,

$$\theta_{lossless} = \frac{s^2}{\mathrm{Nu}_d k_s L A_f} \tag{16}$$

where: Nu_d = 8.235 for fully-developed flow with $H \gg s$

We see that the performance of a lossless heat sink in fully-developed flow depends only on its volume, the fluid thermal conductivity k_s, and the gap s; it is independent of the velocity u and the various other fluid properties (ρ, ν and c_p). Varying the velocity changes the caloric thermal resistance, but the convection term remains unchanged. This can be an important feature, particularly with high heat-capacity fluids (liquids), since heat transfer will be relatively insensitive to velocity. Note that for a given fluid and available heat sink volume, $\theta_{lossless}$ is proportional to the gap s squared. This provides a strong motivation for using the smallest possible gaps in real ducted-flow designs. Typically, manufacturing limitations and limits on fluid power (which determines the mass-flow rate and hence the caloric resistance), will determine the lower bound on s.

2.4 Lossless Heat Sink in Entrance-Region Flow

In Section 1.3, we showed that the entrance-region heat-transfer model can be expected to apply when the fin spacing or gap is large enough that the adjacent developing boundary layers do not meet. This is basically true for any ducted or non-ducted structure if the velocity is high enough. We shall call this the *high-velocity regime*. While we do not yet know the lower limits of this regime, we can nevertheless calculate the thermal resistance of a lossless heat sink at high velocities. Substituting equation (13) into equation (15),

$$\theta_{lossless} = \frac{s}{1.328\,\frac{k_s\sqrt[3]{\mathrm{Pr}}}{\sqrt{\nu}}\,A_f\sqrt{u\,L}} \tag{17}$$

The dependencies here are more complicated than for fully-developed flow. In addition to volume, gap, and thermal conductivity, the entrance-region performance is affected by the length L of the heat sink, the velocity u, and additional fluid properties. Here $\theta_{lossless}$ is proportional to s, rather than s^2 as in the fully-developed case. This is because while reducing fin spacing increases the surface area in both cases, the convection coefficient in the entrance region is independent of the gap, as long as the gap is large enough to preclude boundary-layer interaction. We will show that to function as effective heat sinks, non-ducted structures must be at operated velocities high enough to avoid such interaction.

2.5 High-Velocity Regime

The high-velocity regime is where the entrance-region models apply to both ducted and non-ducted structures. This section examines the lower limits of this high-velocity regime, where the entrance-region models begin to break down due to interaction of adjacent boundary layers. As was shown in Section 1.3, the edge of the boundary layer is defined as the locus of points where the velocity is some given fraction of the free-stream value. This fraction is embodied in the coefficient γ from equation (6) repeated below.

$$\delta = \gamma\sqrt{\nu\,x/u} \tag{18}$$

where:

δ = momentum-boundary-layer thickness, m
γ = boundary-layer thickness parameter, dimensionless
ν = kinematic viscosity, m^2/sec
x = distance from the leading edge of the plate, m
u = free-stream velocity, m/sec

We would expect the entrance-region flow model (and its corresponding heat-transfer equation) to apply when the fins are spaced far enough apart that the adjacent boundary layers do not appreciably interfere. Roughly speaking, for a pair of plates a distance *s* apart, the boundary layers can be said to have met when each has grown to thickness *s*/2 (Figure 2-2).

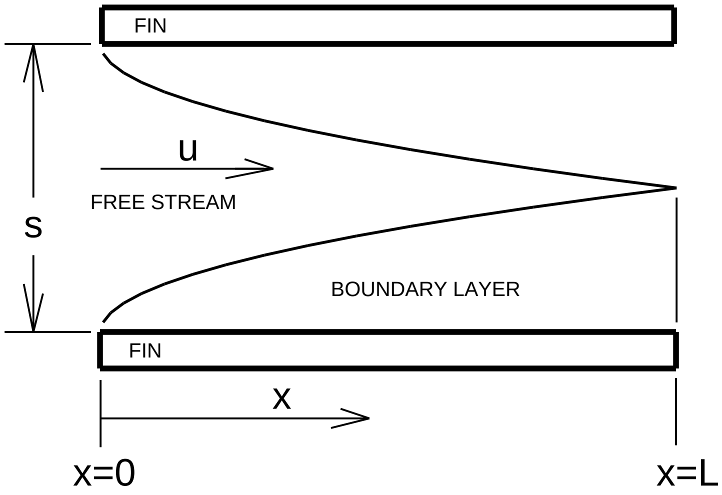

Figure 2-2: Entrance-Region Boundary Layers between Parallel Fins

Thus we expect our entrance-region relations to apply over an entire heat sink when

$$s > 2\gamma\sqrt{\nu x/u} \tag{19}$$

or

$$u > 4\nu L\left(\frac{\gamma}{s}\right)^2$$

This relationship can be used to define a transition velocity *U* above which the entrance-region models are expected to apply. This is not an abrupt transition. The models will apply most accurately at velocities much greater than *U*, less well near *U*, and poorly at velocities well below *U*.

$$U = 4\nu L\left(\frac{\gamma}{s}\right)^2 \tag{20}$$

where: *U* = transition velocity, m/sec

Reported values from the literature for the boundary-layer thickness parameter γ, are presented in the table below.

Varying the geometry and the thickness criterion varies the value of γ. While this bewildering selection may at first seem discouraging, it does let us bound the problem somewhat; values of γ on the order of 5.0 can be expected to give a conservative (high) value for the transition velocity *U*. On the other hand, we would not be surprised if our

Table 2-1: Boundary-Layer Thickness Parameter γ		
γ	***geometry (thickness criterion)***	***Source***
5.83	flat plate (u = free-stream value)	Blasius [1]
5.0	flat plate (u =99% of free-stream value)	White [17]
1.72	flat plate ("displacement thickness")	White [17]
1.118	tube flow (u =98% of free-stream value)	London [14]
1.0	simple diffusion-length model	Tuckerman [15]

entrance-region heat-transfer model was inaccurate in the vicinity of the transition velocity if values of γ of less than one were applied.

2.6 Non-Ducted Structures in Low-Velocity Regime

When the free-stream velocity u is less than the transition velocity U, the heat sink is operating in the low-velocity regime. There are interesting differences between the behavior of ducted and non-ducted structures in the low velocity regime. Where ducting confines the fluid, forcing it to flow between fins, the fully-developed flow models from Sections 1.4 and 2.3 can be expected to apply. They will be most accurate at very low velocities where the flow is fully-developed over most of the length of the duct.

A non-ducted structure behaves very differently in the low-velocity regime. In this case the fluid is free to flow around the heat sink as well as through it and this is exactly what happens! As the free-stream velocity decreases below U, a decreasing fraction of the fluid penetrates the fins and passes through the heat sink. Below the transition velocity, the fluid does not traverse the entire length of the fins, rather it penetrates the fin array some distance before spilling out the ends and around the remainder of the heat sink. The downstream portion of each fin confers little benefit. Lindquist refers to this phenomenon as ‘‘boundary-layer plugging [11].’’ At very low velocities, the flow is almost entirely plugged. The fluid goes around the fins rather than through them. Convection from the heat sink approaches that of a solid block of the same outline dimensions as u goes to zero.

The flow through a non-ducted structure below the transition velocity is highly three-dimensional and difficult to analyze. An intuitive appreciation can be gained from the following example. We consider the outermost fin of an array of flat fins and examine the flow over both its inner and outer surfaces at various velocities. At high velocities, the boundary layers are thin and the flow field over the inside (gap side) of the fin is indistinguishable from that over the outside. Below the transition velocity, symmetry is no longer satisfied. As the boundary layer on the inside of the fin meets and combines with that of its neighbor, the fluid takes the easy way out by going around rather than through the array.

For our purposes there is no need to examine the low-velocity regime for non-ducted flow in great detail. It is sufficient to observe that a non-ducted heat sink will have poor performance at a given velocity if its fins are too close together. This suggests that there is some optimal fin spacing that maximizes surface area while avoiding plugging. The next section will show how this optimal spacing can be approximated. A very simple thermal model for the low-velocity regime in non-ducted flow can be found in Appendix A.

2.7 Optimal Fin Spacing in High-Velocity Regime

The two previous sections suggest that for a non-ducted heat sink operated at some specified fluid velocity u, there is some optimal value for the fin spacing s. Our analysis of the transition velocity suggests that this optimal spacing can be determined from an expression like equation (20). The dimensionless boundary-layer thickness parameter γ must be empirically determined, but based on reported values (Table 2-1) we would expect it to fall somewhere between 1 and 6. Using this effective boundary-layer thickness parameter γ_{eff}, we define:

$$S = 2\gamma_{eff}\sqrt{\nu L/u} \tag{21}$$

where:

S = optimal fin spacing for non-ducted heat sinks, m

γ_{eff} = effective boundary-layer thickness parameter, dimensionless

This problem is not treated adequately in the published literature, so determining an appropriate value of γ_{eff} presented a problem. In the discussion section of a paper by Gardner, Walter Gloyer cites early work by Wagener suggesting the most effective fin spacing in air to be 1.0 to 1.12 times the boundary-layer thickness [4, 16]. Details are sketchy, but the data can be correlated with equation (21) for values of $4 < \gamma_{eff} < 7$. The fins were stubby compared to their ‘‘Teilung’’ (spacing or pitch) and long in the direction of flow, so the boundary layer from the base of the fin array may have been a factor. Schneider suggested that ‘‘tests have shown’’ the optimal fin spacing may be ‘‘as small as 1.12 times the maximum boundary-layer thickness’’, but he neither gave his source nor said how this maximum boundary-layer thickness was defined [13]. I suspect he may have been referring to Wagener’s work. Fox has suggested a value of $\gamma_{eff} = 1.8$ as a fin optimization factor for air [3].

In the absence of any additional data, we provisionally accept Fox's value of γ_{eff}=1.8 for subsequent calculations. We further assume that at this value of γ_{eff}, the entrance-region heat-transfer model will apply. Analysis of data from heat sinks in air, by Lindquist and by Motorola, shows these assumptions to be at least approximately correct: that γ_{eff} is less than two or three respectively [11, 12]. We will also apply this same value to analysis of liquid-cooled non-ducted heat sinks. It is reasonable to expect that γ_{eff} might assume different values because differing fluid properties lead to differing rates of momentum and thermal boundary-layer development (see Appendix B for further discussion). Since this parameter figures heavily in non-ducted heat sink optimization, having a locally valid value is important. This area is a clear candidate for further study.

2.8 Optimal Lossless Heat Sinks for High-Velocity Regime

Armed with our provisional value for γ_{eff}, we proceed directly to the design of optimal lossless non-ducted heat sinks. Substituting the optimal fin-spacing relation, equation (21), into the lossless entrance-region model, equation (16), $\theta_{lossless}$ can be expressed as:

$$\theta_{lossless} = \frac{\gamma_{eff}\,\nu}{0.664\,k_s\sqrt[3]{\mathrm{Pr}}\,A_f\,u} \tag{22}$$

We have constructed a lower bound for the thermal resistance of non-ducted heat sinks based only on the fluid used, its velocity u, and the available frontal area A_f. The lossless thermal resistance is inversely proportional to the velocity u. It is also inversely proportional to the frontal area A_f. It may be surprising that it is independent of the heat sink length L. The heat transfer from an optimal lossless-fin non-ducted heat sink does not depend on its length; it depends only on the correct matching of length and gap! This is because both the fin-spacing relation, equation (21), and the heat-transfer model, equation (16), spring from analysis of a boundary layer that grows as $\sqrt{x}$.

While finite fin conductivities will reintroduce a dependency on length L, this lossless model is a powerful tool for rough-cut system design. For a given required thermal resistance and given chip-package spacing, it provides a lower bound on the board-to-board spacing. It becomes clear why with non-ducted flow at a given free-stream velocity, the board-to-board spacing must increase as the required heat sink resistance is reduced.

2.9 Nusselt-Number Substitution

While they are different, both our entrance-region (high-velocity regime) and fully-developed (low-velocity ducted) models assume a uniform convection coefficient over the entire surface of each fin. A way of relating these two models will prove to be a useful analytical expedient for the coming lossy-fin optimizations; it will allow one set of fin-thickness optimizations to serve both cases. Because of its simpler form, we choose the fully-developed (low-velocity ducted) model as our base case. We thus require for the entrance-region model, an equivalent to the fully-developed Nu_d. This is done by equating $h_{L,average}$ and h_d from equations (11) and (13), then substituting in the optimal spacing from equation (21) and solving for Nu_d.

$$\mathrm{Nu}_d = 2.656\,\gamma_{eff}\sqrt[3]{\mathrm{Pr}} \tag{23}$$

As might be expected, the equivalent Nusselt number depends only on the value assumed for γ_{eff} and on the fluid properties. When applying this equivalent Nu_d to equations for fully-developed flow, it is important to remember that both the Nusselt number substitution and the optimal fin-spacing equation (21) must be used together since our derivation of equation (23) assumed optimal fin spacing. This is illustrated in the design example in Section 3.8.

3

Lossy-Fin Models

3.1 Introduction to Heat Sinks with Lossy Fins

In the previous chapter, optimal heat sinks were developed by assuming that fin conduction plays a negligible role; the fins were assumed to have infinite thermal conductivity and hence zero thickness. We expect this to be a reasonable approximation for real heat sinks when fins are short and thin, fin conductivity is high, and the convection coefficient is low. While our lossless models provide a satisfactory lower bound on heat sink thermal resistance, they seriously overstate the performance of many real designs. Fins with finite thermal conductivity have finite conduction losses and take up a finite amount of space that would otherwise be available to increase surface area.

To develop useful models for lossy-fin heat sinks (Figure 3-1), we first examine a traditional single-fin model and apply it to fin arrays. While direct fin-thickness optimization using this relation requires numerical methods, the relationship can be applied directly to constructing bounding cases that bracket the exact optima where the fin height H is much greater than the gap s. Where the fin height is less, the previously derived lossless case and a simple thin-fin model bracket the optima. These four solutions are normalized by comparing their performance to the lossless case, and recast with dimensionless variables. Together they provide upper and lower performance bounds on the exact optima over the entire design space. Comparing these bounds and noting where they intersect shows the domain over which each is binding. A simple function is then constructed that bounds the optima over the entire domain, enabling conservative estimates of the performance of optimal heat sinks. Section 3.8 is a comprehensive example that illustrates how these bounding models are applied in designing a heat sink. Finally we show how this work relates to the the work of Tuckerman and of Keyes, where fluid power rather than fluid velocity was the basis for optimization [15, 8].

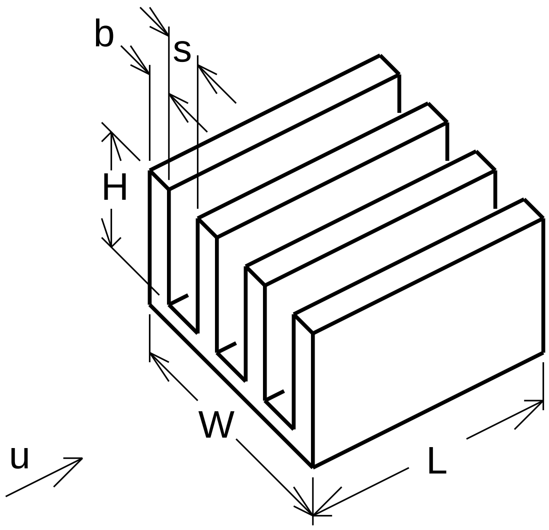

Figure 3-1: Dimensions of Lossy-Fin Heat Sink

3.2 Exact Fin-Thickness Optimization

The thermal resistance of a single fin can be derived by performing an energy balance on a differential volume element. This standard solution can be found in any introductory heat-transfer text [6]. For the case of a rectangular fin with an adiabatic (insulated) tip and uniform convection coefficient, and where the length L is much greater than the thickness b:

$$\theta_{single\,fin} = \frac{1}{L\sqrt{2\,h\,k_b\,b}\;\tanh\left(H\sqrt{2\,h/(k_f\,b)}\right)} \tag{24}$$

where:

$\theta_{single\,fin}$ = exact thermal resistance of a single fin, °C/W
h = convection coefficient, W/(m^2 °C)
k_b = thermal conductivity of fin, W/(m °C)
b = fin thickness, m

This equation can be applied to a fin array (size $H \times W \times L$) with fin spacing s. As described in Section 2.9, asymptotic fully-developed flow will be our base case and the Nusselt number substitution will be used to deal with non-ducted designs. Substituting in for h from equation (11) and combining the individual fin resistances, we have:

$$\theta_{exact} = \frac{s+b}{WL\sqrt{\mathrm{Nu}_d k_b k_s b/s}\ \tanh\left(H\sqrt{\mathrm{Nu}_d k_s/(k_b s b)}\right)} \tag{25}$$

where: θ_{exact} = exact thermal resistance of a fin array, °C/W

This equation is valid for any set of parameters and can be used to accurately calculate the thermal resistance of any given fin array. It can also be used to find the optimal fin thickness B_{exact} by differentiation with respect to b, resulting in:

$$\tanh^2\left(f_1(B_{exact})\right) - \tanh\left(f_1(B_{exact})\right)\frac{f_2(B_{exact})}{f_1(B_{exact})} - 1 = 0 \tag{26}$$

where:

B_{exact} = exact optimal fin thickness, m

$f_1(B_{exact}) = \dfrac{H}{\alpha\sqrt{sB_{exact}}}$, dimensionless

$f_2(B_{exact}) = \dfrac{B_{exact} - s}{B_{exact} + s}$, dimensionless

$\alpha = \sqrt{k_b/(k_s \mathrm{Nu}_d)}$, dimensionless

The exact optimal fin thickness may be found by solving numerically for B_{exact}. While this may be quite reasonable for design of a particular heat sink, in the absence of a closed-form solution, it offers us little insight.

3.3 Lossy Fins of Infinite Height

We can find a lower bound on the thermal resistance of any heat sink having width W and length L by evaluating a heat sink of unbounded height H. Equation (26) shows us that as $H \to \infty$, an optimal design sets $B_{exact} = s$ (remember: $\tanh\infty = 1$). Volume resources are evenly divided between conduction and convection. The optimal fin thickness will **always** be less than the gap for finite fins; this will be exploited in the next section to construct an upper bound. We might expect that as H increases, the thermal resistance will approach some limiting value since the temperature at the end of a long fin approaches that of the surrounding fluid, hence no heat is transferred near the tip. Indeed, for fins of infinite height and optimal thickness, equation (25) reduces to:

$$\theta_{infinite\,fin} = \frac{2s}{WL\sqrt{\mathrm{Nu}_d k_b k_s}} \tag{27}$$

where: $\theta_{infinite\,fin}$ = thermal resistance of optimal design when H unbounded, °C/W

Any heat sink with finite-length fins will of course have worse performance; $\theta_{infinite\,fin}$ is a global lower bound on the thermal resistance. Further insight can be gained by recasting equation (27) into the familiar form $\theta = \frac{1}{h \cdot area}$. Substituting for Nu_d from equation (11) yields:

$$\theta_{infinite\,fin} = \frac{1}{h \cdot area} = \frac{1}{h_d \alpha W L} \tag{28}$$

where:

$\alpha = \sqrt{k_b/(k_s \mathrm{Nu}_d)}$ = maximum increase in effective heat-transfer area, dimensionless

$h_d = \frac{k_s \mathrm{Nu}_d}{2s}$, W/(m^2 °C)

Note that the area is simply the base area ($W \times L$) times α. The dimensionless number α is the maximum enhancement of effective heat-transfer surface area. It is given the distinction of a formal definition because it will pop up frequently in subsequent analysis (in fact it already did, in equation (26)). The magnitude of α is of fundamental importance; if $\alpha < 1$, fins don't help. This situation can occur with the high Nusselt numbers associated with turbulent flow and/or where the ratio k_b/k_s is small. In such cases, fins reduce heat transfer by effectively insulating the portion of the surface they cover.

Example: Is FR-4 (glass/epoxy) useful for non-ducted heat sink fins in a Fluorinert™ FC-77 cooled system?

Material properties for FC-77 and FR-4 are found in Appendix D. Assuming that $\gamma_{eff} = 1.8$, the equivalent Nu_d is found using equation (23);

$$\mathrm{Nu}_d = (2.656)(1.8)\sqrt[3]{23.73} = 13.73.$$

Thus $\alpha = \sqrt{(.26)/(.062 \times 13.73)} = 0.55$.

Since α is less than 1, the fins confer no benefit; the thermal resistance would be lower without them.

3.4 Truncated Fins

We can determine an upper bound on the thermal resistance for optimal heat sinks of finite size by truncating the fins while maintaining the fin thickness equal to the gap. The performance of such a fin array can be calculated from equation (25):

$$\theta_{trunc} = \frac{2s}{WL\sqrt{\mathrm{Nu}_d k_b k_s}\tanh\left(\frac{H}{s\alpha}\right)} \tag{29}$$

where: θ_{trunc} = thermal resistance with truncated fins and $b = s$, °C/W

Note that this is identical to equation (27) with the exception of the hyperbolic tangent. This suggests defining another dimensionless variable, the dimensionless channel height λ.

$$\lambda = \frac{H}{s\alpha} \tag{30}$$

where: λ = dimensionless channel height

If we truncate to some large value of λ, there is little loss of performance. For example, at $\lambda = 1$, θ_{trunc} is 31% higher than our global lower bound $\theta_{infinite\,fin}$. For $\lambda = 2$, the penalty is only 4%. Clearly even when there are no constraints on fin height, there is little reason to make the channels higher than about 2λ. While the performance could be improved by optimizing the fin thickness (by reducing it somewhat), there is relatively little to be gained.

Note that θ_{trunc} decreases along with the gap s. How far the thermal resistance can be reduced is limited only by how well we can miniaturize fin structures and whether or not our pumps are powerful enough to supply the required flow. This will be discussed in more detail in Section 3.9.

3.5 Lossy Thin-Fin Model

The truncated and infinite-fin models provide upper and lower bounds on the thermal resistance of optimal heat sinks. The models closely agree when the dimensionless channel length λ is greater than 1, and they converge for infinitely tall fins. The lossless-fin model provides a global lower bound, and approaches the exact optima as the dimensionless channel length becomes small. The thin-fin model will provide a corresponding upper bound.

Our single-fin model, equation (24), was derived using an energy balance on a differential volume element. This allowed correctly accounting for conduction and convection losses for each slice of the fin, from base to tip. A different approach is used to derive the lossy thin-fin model.

A worst-case fin model assumes that heat must traverse the entire height of the fin before being removed from the sides by convection. It is as if the entire surface of the fin were connected thermally to the fin tip. This overstates actual conduction losses, and is thus consistent with our objective of developing an upper bound. Applying Fourier's Law (equation (1)) to a single fin,

$$\theta_{fin\,conduction} = \frac{H}{k_b b L} \tag{31}$$

where: $\theta_{fin\,conduction}$ = lumped (worst case) single-fin conduction resistance, °C/W

The convective thermal resistance for a single fin is determined by equation (4) and equation (11):

$$\theta_{fin\,convection} = \frac{s}{\mathrm{Nu}_d k_s L H} \tag{32}$$

where: $\theta_{fin\,convection}$ = single-fin convective resistance, °C/W

Adding these two series resistances and dividing by the number of fins yields an upper bound on the thermal resistance of an arbitrary heat sink:

$$\theta_{upper\,bound} = \frac{1}{WL}\left(\frac{Hs}{k_b b} + \frac{bs}{\mathrm{Nu}_d k_s H} + \frac{H}{k_b} + \frac{s^2}{\mathrm{Nu}_d k_s H}\right) \tag{33}$$

where: $\theta_{upper\,bound}$ = upper bound on thermal resistance of arbitrary fin array, °C/W

Note that the third and fourth terms of this equation are independent of the fin thickness b. The third term is the conductive resistance of a rectangular solid $\theta = H/(k_b WL)$ and the fourth term is the expression for a lossless heat sink. We differentiate $\theta_{upper\,bound}$ to find the optimal fin thickness $B_{thin\,fin}$. Since our fin conduction model overstates the fin resistance, $B_{thin\,fin}$ will be greater than B_{exact}.

$$B_{thin\,fin} = \frac{H}{\alpha} \tag{34}$$

where: $B_{thin\,fin}$ = optimal fin thickness for thin fin model, m

This equation may look familiar. Rearranging reveals a dimensionless fin height $H/(B_{thin\,fin}\alpha)$ analogous to the dimensionless channel height λ. Our optimization sets this dimensionless fin height be equal to one; the fin aspect ratio is constant regardless of the other parameters. This is obviously not correct for large λ, since it requires that the fin thickness grow without bound. For small λ, the accuracy of the fin thickness optimization is less important. The fins comprise a relatively small proportion of the heat sink volume, and the thermal resistance approaches that of the lossless case regardless.

Finally, substituting $B_{thin\,fin}$ into our expression for the exact thermal resistance (equation (25)),

$$\theta_{thin\,fin} = \frac{H}{(k_b WL)} \cdot \frac{(1+\lambda)}{(\lambda^{3/2} \tanh \lambda^{1/2})} \tag{35}$$

where: $\theta_{thin\,fin} = \theta_{exact}$ evaluated @ $b = B_{thin\,fin}$, °C/W

3.6 Bounding Models Normalized and Compared

We have constructed two upper bounds and two lower bounds that enclose the optimal thermal resistance for a volume-limited heat sink. One pair of upper and lower bounds converges for channels of large dimensionless height, and the other pair converges for channels of lesser height. To facilitate comparisons we will perform some further non-dimensionalization and normalization. It is most instructive to compare each bounding model to the fully-developed lossless case from Section 2.3.

We recast the fully-developed lossless model (equation (17)) in terms of the dimensionless channel height λ and a normalized thermal resistance Ω. This reduces the equation for $\theta_{lossless}$ to:

$$\theta_{lossless} = \frac{\Omega}{\lambda^2} \tag{36}$$

where: $\Omega = \frac{H}{k_b WL}$ = normalized thermal resistance, °C/W

Note that the normalized thermal resistance represents the conductive resistance of a rectangular solid of height H and base $(W \times L)$. We will compare each model to the lossless case by dividing it by $\theta_{lossless}$ and defining the result to be the effectiveness ratio. Thus by definition,

$$\zeta_{lossless} = 1 \tag{37}$$

where: ζ_{lossless} = effectiveness ratio for lossless model, dimensionless

In a similar manner, we find the effectiveness ratio for each of the other three bounding models. Non-dimensionalizing as required, equations (27), (29), and (35) yield:

$$\zeta_{infinite\,fin} = 2\lambda \tag{38}$$

$$\zeta_{trunc} = \frac{2\lambda}{\tanh\lambda} \tag{39}$$

$$\zeta_{thin\,fin} = \frac{\sqrt{\lambda}(\lambda+1)}{\tanh\sqrt{\lambda}} \tag{40}$$

The closer the effectiveness ratio is to one, the closer the thermal resistance is to that predicted by the lossless model. The thermal resistance for each bounding model can of course be expressed as the product of its corresponding effectiveness ratio and the lossless thermal resistance.

$$\theta_{infinite\,fin} = \frac{2\Omega}{\lambda} \tag{41}$$

$$\theta_{trunc} = \frac{2\Omega}{\lambda\tanh\lambda} \tag{42}$$

$$\theta_{thin\,fin} = \frac{\Omega(\lambda+1)}{\lambda^{3/2}\tanh\sqrt{\lambda}} \tag{43}$$

Figure 3-2 shows the dimensionless channel height λ versus the effectiveness ratio ζ for our four bounding models. Notice that the upper bounds intersect at $\lambda = 1$ and that the lower bounds intersect at $\lambda = 0.5$. Applying each model in the domain where it is the least upper bound or greatest lower bound, we can construct a pair of composite relationships that span the entire domain. Figure 3-3 illustrates the composite least upper bound and greatest lower bound.

The composite upper and lower bounds differ by the greatest amount at $\lambda = 0.5$; the effectiveness ratio of the lower bound is 42.6% less than that of the upper.

Figure 3-2: Dimensionless Channel Height λ *vs.* Effectiveness Ratios ζ for Bounding Models

Figure 3-3: Composite Least Upper and Greatest Lower Bounds

3.7 Global Least Upper Bound for Optimal Thermal Resistance

While the composite upper bound permits conservatively estimating the performance of optimal heat sinks, it has a significant failing. Having two separate equations to cover the entire domain of λ requires knowing which side of $\lambda = 1$ you are on. This is only a minor shortcoming when the data is to be interpreted graphically. It is a much more serious problem when the optimal thermal resistance is to be embedded in subsequent analysis, as will be done in the next chapter on tower heat sinks. In such cases, it is useful to have a single equation that provides a conservative estimate of the thermal resistance over the entire domain of λ.

This is done by finding an expression that is a global upper bound on our composite least upper bound. Ideally it would be close to the composite upper bound for intermediate values of λ and converge toward the bounding cases as $\lambda \to 0$ and $\lambda \to \infty$. One such equation is suggested by inspection of $\zeta_{infinite\,fin}$ and $\zeta_{lossless}$. Adding together these two effectiveness ratios give another effectiveness ratio that we call ζ_{global}.

$$\zeta_{global} = 2\lambda + 1 \tag{44}$$

where: ζ_{global} = effectiveness ratio of global upper bound

Figure 3-4 compares ζ_{global} to our composite least upper bound.

Figure 3-4: Comparing ζ_{global} to Composite Least Upper Bound

A global upper bound on the thermal resistance of an optimal heat sink is thus:

$$\theta_{global} = \frac{\Omega(2\lambda + 1)}{\lambda^2} \tag{45}$$

These functions meet our requirement for a least upper bound valid over the entire domain. Figure 3-5 compares the composite least upper and greatest lower bounds to ζ_{global} over the domain.

Figure 3-5: Ratio of Composite Upper and Lower Bounds to ζ_{global}

As the difference between ζ_{global} and the composite least upper bound never exceeds about 18%, the use of ζ_{global} instead of the more precise bounds is reasonable where an expression valid over the entire domain is required. It can also be seen that ζ_{global} is within a factor of 2 of the greatest lower bound over the entire domain. This constitutes an informal proof that ζ_{global} provides an estimate of the optimal performance that is conservative but is never more than a factor of two off. It may in fact be considerably closer; for proof, solution of equation (26) is required.

3.8 Design Example

This section presents an example to show how the preceding theory can be applied to an actual design. The step-by-step method given is general enough to serve as both an informal review and as a template to apply to other ducted and non-ducted problems. I've included running commentary to drive home many important points common to all heat sink designs.

A large gate-array package and its attached spreader can be modeled as a 40.4 mm (1.59") square heat source. A height of 14.1 mm (0.555") is available above the spreader to accommodate an array 6061-T6 aluminum fins. What is the thermal resistance of an optimal non-ducted heat sink for operation at a minimum air velocity of 4.06 m/sec (800 fpm)?

We will use material properties from Appendix D and assume that $\gamma_{eff} = 1.8$. Since this is a non-ducted design, we first apply equation (23) to determine the equivalent Nusselt number Nu_d .

$$Nu_d = 2.656\, \gamma_{eff} \sqrt[3]{Pr}$$

where:

$Nu_d = 4.26$ = equivalent Nusselt number, dimensionless
$\gamma_{eff} = 1.8$ = effective boundary-layer thickness parameter, dimensionless
$Pr = .708$ = Prandtl number, dimensionless

This equivalent Nusselt number Nu_d will apply to any air-cooled non-ducted design, at any air velocity. If we were instead evaluating a ducted heat sink at low velocity with **any** fluid, we would simply have set $Nu_d = 8.235$.

Solving equation (28) for the maximum effective surface area enhancement α we find that,

$$\alpha = \sqrt{k_b/(k_s\, Nu_d)}$$

where:

$\alpha = 37.53$ = maximum increase in effective heat-transfer area, dimensionless
$k_b = 156.0$ W/(m °C) = thermal conductivity of 6061-T6 aluminum
$k_s = .026$ W/(m °C) = thermal conductivity of air

This parameter tells us how much an optimal heat sink with infinitely high fins would enhance heat transfer from our planar heated surface (Section 3.3). Since α is much greater than 1, a properly designed finned heat sink will indeed reduce the thermal resistance. Note also that this value of α will apply to **any** non-ducted air-cooled heat sink made of 6061-T6 aluminum.

We next use equation (21) to calculate the optimal fin spacing.

$$S = 2\gamma_{eff} \sqrt{\nu L/u}$$

where:

S = 1.47 mm (.058") = optimal fin spacing for non-ducted heat sink
$\nu = 16.8 \cdot 10^{-6}$ m^2/sec = kinematic viscosity of air
$L = 40.4$ mm = heat sink length in direction of flow
$u = 4.06$ m/sec = air velocity

If this had been a ducted rather than a non-ducted design, the fin spacing would have been specified on the basis of pressure drop or manufacturing constraints.

We can now use equation (30) to find the dimensionless channel height λ.

$$\lambda = \frac{H}{s\alpha}$$

where:

λ = .256 = dimensionless channel height
H = 14.1 mm = fin height
$s = S$ = 1.47 mm = fin gap

This small dimensionless channel height ($\lambda < 1$) tells us we're in the regime where the performance of our heat sink approaches that of the lossless case and that if more height were available, it could be effectively used to further reduce the thermal resistance.

Equation (36) gives us the normalized thermal resistance Ω and the thermal resistance $\theta_{lossless}$ for the lossless fin case.

$$\Omega = \frac{H}{k_b W L}$$

where:

Ω = .0554 °C/W = normalized thermal resistance
W = 40.4 mm = heat sink width

and,

$$\theta_{lossless} = \frac{\Omega}{\lambda^2}$$

where: $\theta_{lossless}$ = .845 °C/W = thermal resistance of optimal lossless heat sink

$\theta_{lossless}$ could have been obtained directly from equation (22), but by following this route, we have already determined other relevant parameters and can proceed directly to analysis of the lossy-fin case. Equation (36) however conceals the fact that for optimal non-ducted heat sinks, $\theta_{lossless}$ is inversely proportional to the frontal area and depends not a whit on the length L (Section 2.8). This is not true for the ducted case, where $\theta_{lossless}$ is inversely proportional to the volume.

The thermal resistance of an optimal lossy-fin heat sink is found by multiplying $\theta_{lossless}$ by some effectiveness ratio ζ (Section 3.6). The most general solution is our global upper bound ζ_{global} (equation (44)).

$$\theta_{global} = \zeta_{global} \cdot \theta_{lossless}$$

where:

θ_{global} = 1.28 °C/W = global upper bound on thermal resistance of an optimal heat sink

$\zeta_{global} = 2\,\lambda + 1$
= 1.512 = effectiveness ratio of global upper bound, dimensionless

Since the dimensionless channel height λ is less than 1, the thin-fin model (equation (40)) will offer an improved (though still conservative) estimate.

$$\theta_{thin\,fin} = \zeta_{thin\,fin} \cdot \theta_{lossless}$$

where:

$\theta_{thin\,fin}$ = 1.15 °C/W = thin-fin model upper bound on thermal resistance of optimal heat sink

$\zeta_{thin\,fin} = \dfrac{\sqrt{\lambda}\,(\lambda + 1)}{\tanh \sqrt{\lambda}}$
= 1.361 = effectiveness ratio of thin-fin model

If we actually want to build such a heat sink, equation (34) gives the optimal fin thickness in this regime.

$$B_{thin\,fin} = \frac{H}{\alpha}$$

where: $B_{thin\,fin}$ = .37 mm (.015") = optimal fin thickness for thin-fin model

Remember that the actual optimal fin thickness will be somewhat less, though when λ is small there is little difference (Section 3.5). When λ is greater than 1, the optimal fin thickness is approximately equal to the gap (Section 3.4).

In conclusion, the optimal aluminum heat sink will have fins .37 mm (.015") thick and spaced 1.47 mm (.058") apart. Its thermal resistance in a 4 m/sec (800 fpm) airflow will be less than 1.15 °C/W.

3.9 Design for Minimum Pumping Power

We have so far focused entirely on optimizing heat sinks based on a fixed fluid velocity and a fixed heat sink volume. This completely ignores the issue of efficiency: the watts of pumping power expended to remove a watt of heat from the chip. While efficiency is not usually a constraint for a supercomputer, it can be important in other applications.

We saw in Section 3.4 that if we build a heat sink with equal fin thickness and gap $b = s$, and truncate the fins to some large value of λ, there is little loss of performance. For example, at $\lambda = 1$, the thermal resistance is 31% higher than $\theta_{infinite\,fin}$, and at $\lambda = 2$, the penalty is only 4%. Clearly there is little reason thermally to make the channels much higher than 2λ, and there is a cost in efficiency for overly tall fins. When other parameters are fixed, the fluid power is proportional to the fin height H, so there is an incentive to keep the fins short. Tuckerman's fluid-power-minimizing solutions yielded a dimensionless channel height λ on the order of one or two [15]. Since θ decreases along with the gap s, such a heat sink can be roughly designed by fixing λ in this range and reducing the gap s until the limit of the fluid power or caloric resistance budget is reached. How far the thermal resistance can be reduced is limited only by how well we can miniaturize fin structures and whether or not our pumps are powerful enough to supply the required flow.

Tuckerman performed analysis and experiments on heat sinks in this regime [15]. He focused on power and pressure limited systems and tested ducted micro-channel ($s \approx 50$ microns) heat sinks machined from silicon. Thermal resistances under $0.1\ \mathrm{cm}^2\,°\mathrm{C/W}$ were reported using water with pressure drops on the order of 3 atmospheres. This thermal performance is an order of magnitude better than most systems now under consideration will require. Goldberg explored air cooling with small ducted heat exchangers [5]. Using equal gap and fin thickness as low as 127 microns, with copper fins 12.7 mm high, he obtained thermal resistances on the order of $1 - 2\ \mathrm{cm}^2\,°\mathrm{C/W}$. The manufacturing of these kinds of heat sinks can be as important an issue as fluid power. Machining and molding processes are typically limited to aspect ratios*** of around 10:1 to 20:1. Such processes are well matched to material systems such as silicon/water where the small thermal conductivity ratio k_b / k_s means that there is little benefit to tall fins. For the copper/air system with its higher conductivity ratio, much higher aspect ratios are desirable. This suggests more complicated and expensive corrugated or discrete fin structures. High aspect-ratio fins are also fragile and susceptible to damage. These can both be important practical considerations in air cooled systems.

***Channel aspect ratio = H/s, fin aspect ratio = H/b.

Example: What range of fin or channel aspect ratios is needed for optimal-efficiency ducted water-cooled silicon heat sinks? For air-cooled copper heat sinks? For air-cooled 6061-T6 aluminum heat sinks?

Material properties are found in Appendix D. Assume that the optimal dimensionless channel height λ is 2. We showed earlier that in this regime, the optimal fin thickness is approximately the same as the gap so the fin and the channel aspect ratios will be nearly equal. Solving equation (30) for the channel aspect ratio H/s we find that,

$$\frac{H}{s} = \lambda\alpha.$$

By equation (28), $\alpha = (k_b/(k_s \mathrm{Nu}_d))$, and for tall fins $\mathrm{Nu}_d = 8.235$.**** Thus

$$\frac{H}{s} = \lambda\sqrt{k_b/(k_s \mathrm{Nu}_d)}.$$

For silicon/water: $\frac{H}{s} = (2)\sqrt{(153)/(.61 \times 8.235)} = 11$

For copper/air: $\frac{H}{s} = (2)\sqrt{(381)/(.026 \times 8.235)} = 84$

For aluminum/air: $\frac{H}{s} = (2)\sqrt{(156)/(.026 \times 8.235)} = 54$

Water-cooled silicon heat sinks are within the range where they can be fabricated by a variety of processes. The air-cooled copper structures clearly cannot be so easily built. Even with 6061-T6 aluminum, optimal-efficiency heat sinks for air cooling have to be assembled rather than machined or extruded.

****Remember that the Nusselt number is a function of H/s. Use of the asymptotic value $\mathrm{Nu}_d = 8.235$ can lead to significant errors (>10%) when $L/s < 10$. See Appendix C for details.

4

Tower Heat Sinks

4.1 Benefits of Lateral Spreading

We have thus far in our analysis ignored any consequences of spreading resistance. In previous sections, we assumed that the heat source was a rectangular surface of fixed size, and that the volume available for the heat sink was limited to a bounding box of some height above the surface. Where the heat sources occupy most of a circuit board, these assumptions make sense since the only direction for the heat sinks to grow is up.

For less densely-populated boards, and for chip packages that are significantly larger than the chip, spreading can be exploited in two possible ways: with heat spreaders and/or with tower heat sinks. First, the chip or die can be attached to a substrate that increases the area available for subsequent heat removal. These spreaders can be made from high thermal-conductivity materials to effect as much as a 3× to 4× increase in area with little additional conduction loss. They function as an area to heat-flux transformer. An example is the package for the Motorola MCA2500 gate array [12]. A die approximately 6.8 mm square is bonded to a 15.9 mm diameter BeO (beryllia) spreader that forms an outer surface of the package. For our purposes, such spreaders may be considered an integral part of a given chip-package design; the specification cannot easily be changed by the system designer. If the spreader size is close to that of the overall package outline, and if the packages densely populate the board, the heat sink models of the previous section remain applicable.

If however, the spreader (or the effective spreader area) is appreciably smaller than the package outline, the volume above this additional area might be filled with fins by designing heat sinks that incorporate spreading. Such a design will be called a *tower heat sink*. It may be possible to design a tower heat sink that imposes less of a board-to-board spacing penalty than a non-tower design. This is indeed the case with the current crop of air-cooled ECL gate arrays in single-chip packages.

Following are some rudimentary models that can be used for estimating the performance limits of towers, assessing whether or not towers are likely to be useful in a particular case, and determining the approximate performance of optimal tower designs. These models are very preliminary. With additional work, they could be further improved and refined.

4.2 Spined Tower with Unbounded Frontal Area

For a rectangular heat source of length L and width m, we can evaluate the performance of a tower heat sink of finite length L and infinite frontal area. We'll assume that the tower consists of a central spine of width m, with a fin array extending at a right angles to the spine on each side (Figure 4-1). By assuming piecewise one-dimensional heat flow (up the spine, right angle turn, out the fin), our previous lossy-fin work can be applied. We can calculate a value for the maximum effective surface-area enhancement α for the side-fin arrays using equation (28). This allows us to determine the heat transfer from the spine without getting tangled up in the details of convection from the fins. Treating the spine as a body without fins, its effective convection coefficient is simply the average fin convection coefficient $h_{average}$ times α. Equation (24) for a single fin is then applied to the spine to find the total thermal resistance of the unbounded tower.

$$\theta_{unbounded\,tower} = \frac{s^{1/2}}{L\,k_b^{3/4}\,k_s^{1/4}\,\mathrm{Nu}_d^{1/4}\,m^{1/2}} \tag{46}$$

where:

$\theta_{unbounded\,tower}$ = thermal resistance of spined tower of unbounded frontal area, °C/W

m = width of heat source and heat sink spine, m

Equation (46) can be applied directly to ducted designs. It can of course also be used for the non-ducted case by substituting in the optimal fin spacing for s and the equivalent Nusselt number for Nu_d. Any tower heat sink with finite frontal area will have a higher thermal resistance.

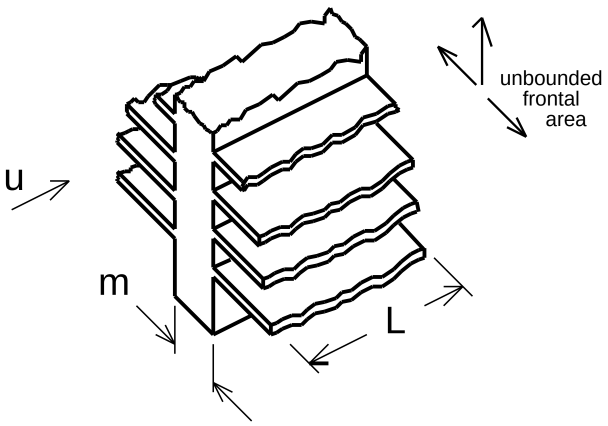

Figure 4-1: Lossy Tower with Unbounded Frontal Area

4.3 Determining When a Tower May be Advantageous

We now have two models for heat sinks of unbounded dimensions: $\theta_{infinite\,fin}$ (equation (28)) for heat sinks of unbounded height, and $\theta_{unbounded\ tower}$ for heat sinks of unbounded frontal area. It is instructive to compare these two models to determine when a tower might be advantageous. We might expect a result analogous to our findings in Section 3.2 where we determined that fins confer no advantage when $\alpha < 1$. Equating $\theta_{unbounded\,tower}$ to $\theta_{infinite\,fin}$, we find the breakeven point.

$$\frac{\alpha \cdot 4s}{m} = 1 \tag{47}$$

We see that an unbounded tower is better than an infinite fin design only when $\alpha \cdot 4s/m > 1$. The tower is worse when the fin spacing s is much less that the heat source width m. It should be no surprise that the proportionality constant includes the maximum effective surface-area enhancement α. α must, of course, still be greater than 1 for fins to be effective.

While equation (47) is a useful guide for many finite-fin problems, there are ambiguities in its application. A comparison will depend on whether height or width is the binding constraint. The model breaks down as the permissible heat sink width approaches the source width m; the spine takes up most of the heat sink volume leaving little room for fins. Also, in many cases a spreader plate of high thermal conductivity can be used to increase the effective width of the heat source to some value greater than m. This might make a non-tower design attractive; there is a tradeoff between the volume and thermal resistance of the spreader and the additional fin volume due to the increased width. Modeling spreader plates cannot be done with our simple one-dimensional conduction models. These various ambiguities can be alleviated somewhat by comparing an optimal non-tower with an optimal tower designed using the results of the next section.

4.4 Finite Spined Tower

Finite spined towers (Figure 4-2) can be analyzed in a manner similar to that used in Section 3.5 to derive the lossy thin-fin model. The lumped resistance for the spine is taken to be its entire conductive resistance from base to tip, as if the base of each fin were connected thermally with the tip of the spine. As before, this is a conservative assumption; it overstates conduction losses in the spine. Here optimal fins are assumed to fill the entire allotted volume ($L \times M \times W$), with the exception of the centrally-located spine of width m. An optimal value for m is found that minimizes the total thermal resistance. Another conservative assumption is made; ζ_{global} is initially assumed to have a fixed value and is evaluated at $H = M/2$.

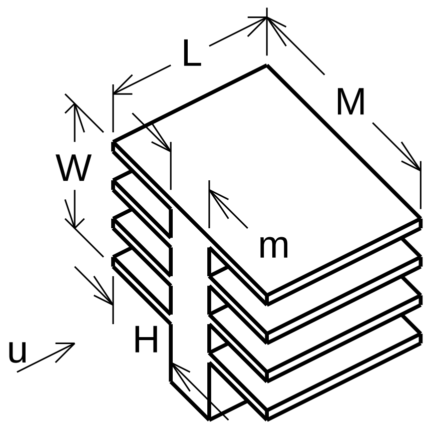

Figure 4-2: Tower Heat Sink Dimensions

Using these approximations, we calculate the resistance for a finite tower of arbitrary spine width.

$$\theta = \theta_{spine} + \theta_{fins} = \frac{W}{k_b m L} + \zeta_{global}\,\theta_{lossless} \tag{48}$$
$$= \frac{W}{k_b L}\left(\frac{1}{m} + \frac{1}{\psi^2 (M+m)}\right)$$

where:

$\psi = \dfrac{W}{\alpha\, s \sqrt{\zeta_{global}}}$ = tower parameter, dimensionless

$\theta_{lossless} = \dfrac{s^2}{\mathrm{Nu}_d\, k_s\, L\, W (M-m)}$

M = overall heat sink width, m

Differentiating to find the optimal spine width m,

$$m = \frac{M\psi}{\psi + 1} \tag{49}$$

Substituting the optimal spine width m back into equation (48) gives,

$$\theta_{finite\,tower} = \frac{W}{k_b L M}\left(1 + \frac{2}{\psi} + \frac{1}{\psi^2}\right) \tag{50}$$

where: $\theta_{finite\,tower}$ = total resistance of optimal finite spined tower, °C/W

The height H of the fins is,

$$H = \frac{M}{2}\,\frac{1}{\psi + 1} \tag{51}$$

Because our conservative model overstates lumped spine resistance, accurate results can be expected only for relatively short towers. $\theta_{spine} = \theta_{fins}$ when $\psi = 1$; we thus expect accurate results only when ψ is less than 1.

Note again that the spine width m is a dependent variable; no account is made for the actual size of the heat source. This ignores 3-d effects such as spreading within the spine and can be a significant source of error in some designs.

If desired, the results can be checked and a more accurate estimate made by iterating using the derived value of H in evaluating ζ_{global}. If the spine is thin ($m \ll M$), this will make little difference.

4.5 Omnidirectional Towers

Our spined tower is a directional heat sink. Omni-directional heat sinks are popular because they can be mounted to a chip package in any orientation without regard for the direction of airflow. One familiar style looks like a set of dinner plates stacked on a post. A spined heat sink can be converted into an omnidirectional design by collapsing the spine into a square or round post of identical cross-sectional area. This condition is satisfied for a square post of side length *P* when,

$$P = \sqrt{mL} \tag{52}$$

where: P = length of side of square post

Similar approximations can be made for cylindrical post heat sinks such as are machined by turning on a lathe. Although the actual flow field around an omnidirectional tower heat sink is three-dimensional, test data indicates that it may be reasonable to just ignore the post, and to calculate the thermal resistance as though the heat sink were a spined tower [11, 12].

Acknowledgments

I am indebted Scott Nettles, who reviewed several drafts of my manuscript. His well targeted comments had a significant influence on the content and organization of this work. My thanks to Brian Reid whose editing efforts greatly enhanced the readability of the the final article. Thanks also to Jack Berenholz, Rob Brownell, Les Fox, Gary Kromann, and Steve Lindquist for getting me off to a solid start in understanding non-ducted flow and supplying many of the references. Les and Steve also looked over my final draft and provided many helpful comments.

References

[1] H. Blasius.
Grenzschichten in Flüssigkeiten mit Kleiner Reibung.
Zeit. Math. Phys. 56(1), 1908.
Cited in 4.

[2] R.D. Danielson.
Cooling a Superfast Computer.
Electronic Packaging and Production :44-45, July, 1986.

[3] L.R. Fox.
Heat Sinks.
Digital Equipment Corporation, Interoffice Memo, 17 May 1985.

[4] K.A. Gardner.
Efficiency of Extended Surfaces.
Trans. ASME 67(1), 1945.
Reprinted with erratum in ASME HTD Vol. 57, 1986, pp. 23-33.

[5] N. Goldberg.
Narrow Channel Forced Air Heat Sink.
IEEE Trans. Components, Hybrids, and Manufacturing Technology CHMT-7(1), March, 1984.

[6] J.P. Holman.
Heat Transfer.
McGraw-Hill, New York, 1976.
ISBN 0-07-029598-0.

[7] M.K. Kayes and Michael E. Crawford.
Convective Heat and Mass Transfer.
McGraw-Hill, New York, 1980.
ISBN 0-07-033457-9. See in particular chapters 6 and 9. Cited in 15.

[8] R.W. Keyes.
Heat Transfer in Forced Convection Through Fins.
IEEE Trans. Electron Devices ED-31(9), September, 1984.

[9] T. Kishimoto *et al.*.
Gas Cooling Enhancement Technology for Integrated Circuit Chips.
IEEE Trans. Components, Hybrids, and Manufacturing Technology CHMT-7(3), Sept, 1984.

[10] A.D. Kraus and A. Bar-Cohen.
Thermal Analysis and Control of Electronic Equipment.
Hemisphere/McGraw-Hill, New York, 1983.
ISBN 0-07-035416-2.

[11] S. Lindquist.
[Gate Array] Heatsink Summary.
Digital Equipment Corporation, Interoffice Memo, 18 July 1986.

[12] *Motorola MCA2500ECL Macrocell Array Design Manual (preliminary)*
Motorola, Inc., 1984.

[13] P.J. Schneider.
Conduction Heat Transfer.
Addison-Wesley, Cambridge, Mass., 1955.

[14] R.K. Shah and A.L. London.
Advances in Heat Transfer. Volume Supplement I: *Laminar Flow Forced Convection in Ducts.*
Academic Press, New York, 1978.
ISBN 0-12-020051-1. Cited in 15.

[15] D.B. Tuckerman.
Heat Transfer Microstructures for Integrated Circuits.
PhD thesis, Stanford University, February, 1984.

[16] G. Wagener.
Der Wärmeuebergang an Kühlrippen.
Beheifte zum Gesundheits Inginieur 1(24), 1929.
Cited in 4.

[17] F. White.
Viscous Fluid Flow.
McGraw-Hill, New York, 1974.
ISBN 07-069710-8.

[18] R.A. Wirtz and P. Dykshoorn.
Heat Transfer from Arrays of Flat Packs in a Channel Flow.
In *Proceedings of the 4th Annual International Electronics Packaging Conference*. October, 1984.

Appendix

A. Thermal Performance of Non-Ducted Heat Sinks in Low-Velocity Regime

Modeling non-ducted heat sinks below the transition velocity U is a difficult problem (See Section 2.6). The fluid is not confined to flow between the fins, and is free to spill out past the fin tips as it encounters the fully-developing velocity profile. The flow becomes more three-dimensional. Our simple two-dimensional models do not hold up; both the entrance-region model and the ducted fully-developed model prove to be optimistic. While we would not purposely design a non-ducted heat sink to be operated in this regime, it would be useful to have a way of predicting its performance.

A simple model for this case can be based on the entrance-region model. The assumption made is that the entrance-region model applies up to the point that the boundary layers meet. Beyond that point, we'll assume that no heat transfer takes place. Physically this can be thought of as accounting for the transition from an internal flow (through the fins) to an external flow (around the heatsink) without worrying about the details of how the fluid mass escapes the fins.

$$h_{L,average} = \frac{0.664\, k_s \sqrt[3]{Pr}}{\sqrt{\nu}} \cdot \frac{u^{3/2}}{U\sqrt{L}} \qquad (53)$$

This model shows reasonable agreement with test data in air [11, 12]. It should however be noted that it is sensitive to the value of U, which is in turn a function of the empirical constant γ_{eff}. Because of its shaky theoretical foundation, the value of this expression is rather limited. It does however indicate how the higher exponent on u in this region drives us to space our fins so that $u > U$ over the range of anticipated flow velocities; fin spacings should be optimized for the lowest anticipated fluid velocity.

B. Comparing Entrance-Region and Fully-Developed Models at the Transition Velocity

The calculation of the equivalent Nu_d suggests an interesting comparison. The non-ducted model presumes that entrance conditions prevail over the entire length of the duct. The fully-developed or ducted models assume an asymptotic-fully-developed flow over the entire duct. For an actual non-ducted heat sink being operated at $u = U$, we might expect little change in the heat transfer if the fins were enclosed to transform it into a ducted design, so ideally both the ducted and the non-ducted models should give the same results at $u = U$. Letting $\mathrm{Nu}_d = 8.235$ and $\gamma = 1.8$, we can solve equation (23) for the Prandtl number.

$$\mathrm{Pr} = 5.1 \tag{54}$$

Both models thus give the same result at the transition velocity when the Prandtl number is 5.1. When the Prandtl number is less than 5.1, the ducted model predicts a higher thermal resistance than the non-ducted model at $u = U$.

This sort of behavior is not surprising; it relates to assumptions made in deriving the models. The first is the use of the asymptotic minimum Nu_d rather than the actual average Nu_d in the ducted flow model. This understates the performance of the ducted model when applied to short ducts. Most experimental correlations for predicting average Nu_d for a short duct apply a dimensionless duct length $L/(s\,\mathrm{Re}\,\mathrm{Pr})$ as a parameter. A more detailed analysis applies these short duct corrections [15].

A second simplifying assumption can be understood by noting that the fluid's thermal conductivity k is the only fluid property that affects the ducted model. In contrast, the non-ducted or entrance-region optimization depends on several additional parameters: the kinematic viscosity ν, the specific heat c_p, and the density ρ as well as the semi-empirical constant γ_{eff}. Remember also that our use of a particular value of γ_{eff} embodies two separate assumptions: that γ_{eff} determines the optimal fin spacing, and that the simple flat-plate heat-transfer model will accurately apply at that spacing. The reason for this was hinted at earlier. A detailed analysis must account for the development of two separate boundary layers, thermal and momentum. Whether the thermal boundary layer develops more or less rapidly than the momentum layer depends on the fluid's Prandtl number [6]. The relationship of their relative thicknesses is given approximately by

$$\delta_{thermal} = \frac{\delta}{\sqrt[3]{\mathrm{Pr}}} \tag{55}$$

where:

$\delta_{thermal}$ = thermal boundary-layer thickness, m
δ = momentum boundary-layer thickness, m

For air with $\mathrm{Pr} \approx 0.7$, the thicknesses are about the same; for Fluorinert FC-77 ($\mathrm{Pr} \approx 24$) and other non-metallic liquids, the thermal layer is the thinner of the two (see Appendix D for fluid properties). Since the optimal fin spacing was based on the development of the momentum boundary layer, we would expect that for Fluorinert and other large-Pr fluids, the flat-plate heat-transfer model will prove accurate at the optimal fin spacing. It is with air, and its more rapidly developing thermal boundary layer, that inaccuracies in heat-transfer calculations might be expected to to be encountered at the optimal fin spacing. Since my provisional value for γ_{eff} was based on experimental data in air, it would not be at all surprising to find that a different value is appropriate for higher Prandtl-number fluids.

Given the differences in our analytical approaches to the ducted and non-ducted problems, we should not expect to be able to directly compare their results in the vicinity of $u = U$.

C. Nusselt Numbers for Rectangular Ducts

Figure 1: Nusselt Numbers for Rectangular Ducts

Figure 1 is copied from Tuckerman's thesis [15]. It gives uniform-flux Nusselt numbers for fully-developed flow in rectangular ducts, with one or more walls transferring heat; Nu is based on *wetted* perimeter (figure courtesy of A. L. London [14]).

D. Material Properties

Listed below are properties for a number of materials that may be useful to the designer. The coolant used in the Cray 2 computer, 3m Corporation's Fluorinert™ FC-77 has been included along with water and the ever-popular air [2]. A number of useful fin and spreader materials are listed along with FR-4, which is lousy for fins, as is demonstrated by the example on page 28 [10]. All properties are at 25 °C.

Table D-1: Fluid Properties

property	***dimension***		**Air**	**FC-77**	**Water**
k_s	W/(m °C)		.026	.062	.61
ν	m^2/sec		$16.8 \cdot 10^{-6}$	$0.8 \cdot 10^{-6}$	$0.9 \cdot 10^{-6}$
ρ	kg/m^3		1.18	1780	1000
c_p	(W sec)/(m °C)		1006	1050	4180
Pr	$\nu \rho c_p / k$ (dimensionless)		.708	23.73	6.13
Boiling pt	°C		<< 0	97	100

Table D-2: Solid Properties

material	***composition***	k_b (W/(m °C))
FR-4		0.26
Alumina	90% Al_2O_3	12.1
Kovar		15.6
Alumina	96% Al_2O_3	29.4
Molybdenum		134.0
Silicon		153.0
Beryllia	95% BeO	156.0
Aluminum	6061-T6	156.0
Aluminum	Pure	216.0
Beryllia	99.5% BeO	242.0
Copper	Pure	381.0

E. List of Symbols

Table E-1: Roman Letter Symbols

Name	***dimension***	***description***
dim	m	characteristic dimension
$f_1(\mathrm{B}_{\mathrm{exact}})$	dimensionless	$H/(\alpha\sqrt{sB_{exact}})$
$f_2(\mathrm{B}_{\mathrm{exact}})$	dimensionless	$(B_{exact} - s)/(B_{exact} + s)$
A	m^2	area normal to the direction of heat flow
A_f	m^2	$H \times W$ = frontal area
A_h	m^2	surface area for convection
$B_{thin\ fin}$	m	optimal fin thickness for thin fin model
B_{exact}	m	exact optimal fin thickness
H	m	fin height
H	m	height in direction of heat flow
L	m	length of the fins in the direction of flow
M	m	overall width of tower heat sink
Nu_d	dimensionless	duct Nusselt number = 8.235 for fully developed flow where $H >> s$
Pr	dimensionless	$\nu\rho c_p / k_s$ = Prandtl number
Re	dimensionless	$dim \cdot u / \nu$ = Reynolds number
S	m	optimal fin spacing for non-ducted heat sinks
U	m/sec	transition velocity
W	m	heat sink width
b	m	fin thickness
c_p	(W sec)/(Kg °C)	heat capacity
d	m	duct hydraulic diameter
f	m^3/sec	volume flow rate
h	W/(m^2 °C)	convection coefficient
$h_{L,average}$	W/(m^2 °C)	average plate convection coefficient
$h_{average}$	W/(m^2 °C)	average convection coefficient
h_d	W/(m^2 °C)	duct convection coefficient
h_x	W/(m^2 °C)	local plate convection coefficient
k	W/(m °C)	thermal conductivity
k_b	W/(m °C)	thermal conductivity of fin
k_s	W/(m °C)	fluid thermal conductivity
m	m	width of heat source and heat sink spine
q	W	heat flow (total heat transfer rate)
s	m	fin gap
u	m/sec	free stream velocity
x	m	distance from the leading edge of the plate

Table E-2: Greek Letter Symbols		
Name	***dimension***	***description***
ΔT	°C	temperature difference (depends on context)
Ω	°C/W	$H/(k_b W L)$ = normalized thermal resistance
α	dimensionless	$\sqrt{k_b/(k_s Nu_d)}$ = max. increase in effective heat transfer area
δ	m	momentum boundary layer thickness
γ	dimensionless	boundary layer thickness parameter
γ_{eff}	dimensionless	effective boundary layer thickness parameter
λ	dimensionless	channel height
ν	m^2/sec	kinematic viscosity
θ	°C/W	thermal resistance
$\theta_{conduction}$	°C/W	conduction thermal resistance
$\theta_{convection}$	°C/W	convection thermal resistance
θ_{exact}	°C/W	exact thermal resistance of a fin array
$\theta_{fin\ conduction}$	°C/W	lumped (worst case) single fin conduction resistance
$\theta_{fin\ convection}$	°C/W	single fin convective resistance
$\theta_{finite\ tower}$	°C/W	total resistance of optimal finite spined tower
θ_{global}	°C/W	global upper bound on thermal resistance of optimal heat sink
$\theta_{infinite\ fin}$	°C/W	thermal resistance of optimal design when H is unbounded
$\theta_{lossless}$	°C/W	thermal resistance of lossless heat sink
$\theta_{single\ fin}$	°C/W	exact thermal resistance of a single fin
$\theta_{thin\ fin}$	°C/W	θ_{exact} evaluated at $b = B_{thin\ fin}$
θ_{trunc}	°C/W	thermal resistance with truncated fins and b = s
$\theta_{unbounded\ tower}$	°C/W	thermal resistance of spined tower of unbounded frontal area
$\theta_{upper\ bound}$	°C/W	upper bound on thermal resistance of arbitrary fin array
ρ	kg/m^3	density
ρc_p	(W sec)/(m^3 °C)	volumetric heat capacity of the fluid
ψ	dimensionless	$W/(\alpha s \sqrt{\zeta_{global}})$ = tower parameter
ζ	dimensionless	effectiveness ratio (for various models)

Table of Contents

List of Figures

List of Tables